PCCP

Accepted Manuscript

ROYAL SOCIETY OF CHEMISTRY

www.rsc.org/pccp

Journal Name

RSCPublishing

ARTICLE

Loading of ionic compounds into metal-organic frameworks: A joint theoretical and experimental study for the case of La^{3+}

Cite this: DOI: 10.1039/x0xx00000x

Received 00th January 2012,
Accepted 00th January 2012

DOI: 10.1039/x0xx00000x

www.rsc.org/

Wei Guo[a], Jinxuan Liu[a], Peter G. Weidler[a], Jianxi Liu[a], Tobias Neumann[b], Denis Danilov[b], Wolfgang Wenzel[b], Claus Feldmann[c] and Christof Wöll*[a]

Crystalline, highly orientated surface-anchored MOF thin films, grown on Au substrates were prepared using liquid-phase epitaxy (LPE). The successful loading of La^{3+} ions into the $Cu_3(BTC)_2$ (HKUST-1) SURMOFs (surface-mounted metal-organic frameworks) was monitored using x-ray diffraction (XRD). Theoretical calculations using classical force-field based Monte Carlo simulations yield a structure with two La^{3+} ions within the large $Cu_3(BTC)_2$ pores, in full agreement with a experimental results on the composition of these films and the relative intensities of the XRD peaks. Implications of these findings for using MOF thin films for electronic applications are briefly discussed.

Introduction

Among highly porous crystalline materials, presently metal−organic frameworks (MOFs)[1-3] see a still increasing amount of attention resulting from their flexible pore sizes and large loading capacity for guest species,[4] in particular metals and metal ions.[5] During the past decade, a huge number of metals@MOFs systems (for metals like Au,[6] Zn,[7] Pd[8]) has been reported, with the metal guests rendering fascinating properties [e.g., such as hydrogen storage,[9, 10] catalysis (e.g. CO oxidation,[11, 12] alcohol oxidation[13])] to the host MOF material. Particularly attractive are the cases where the loading of the metal guest species does change the crystal structure of the host material but only modifies their properties (e.g. electrical conductivity,[14] capacity for ions absorption,[15] optical properties.[16, 17] For a number of applications, e.g. electric/electronic devices,[18] information storage,[19] electro chemistry,[20] heterogeneous catalyst,[21] MOF thin films[22, 23] and the ability to load this MOF-coatings with metals are important.

In the present work we focus on a special type of MOF coatings, surface-mounted metal-organic frameworks (SURMOFs). They represent a particularly important class of MOF thin films since they are crystalline, oriented and exhibit a well-defined thickness. They can be manufactured with thicknesses in the micrometer-regime, allowing the application of standard methods to determine their mechanical,[24] optical[17] and electrical and electrochemical[14, 20] properties. The loading of Eu^{3+} ions into HKUST-I SURMOFs has been shown to result in interesting optical properties, it could be shown that optical excitations resulting from absorption in the MOF ligands could be transferred to the embedded Eu ions.[25]

In the present paper we investigate the loading of La^{3+} cations into HKUST-1 or $Cu_3(BTC)_2$, (BTC, 1,3,5-Benzenetricarboxylic acid), a popular MOF-materials with fairly large (~1nm) pore sizes.[26] Since we target applications in electrochemistry, information storage and sensorics, here we focus on MOF thin films, SURMOFs. Investigations are carried out used x-ray diffraction (XRD), while quantitative information of the Cu/La-ratio is obtained from ICP-OES (Inductively Coupled Plasma Optical Emission Spectrometry) and XPS (X-ray Photoelectron Spectrum) data. In addition, force-field calculations are carried out to obtain the precise positions of the metal cations and their corresponding counter ions in the lattice. Interestingly, these calculations reveal a rather pronounced binding energy of the metal ions within the MOF cavities brought about by the fairly substantial cations BTC ligand interaction. Knowledge about the precise structure of metal ion-loaded MOF thin films is crucial for understanding electrical transport[14], electrochemical behaviour[20] and metal ion diffusion[19] in MOFs and SURMOFs

Experimental

Preparation of Gold Substrates

Gold substrates were obtained from PVD Beschichtungen (Silz, Germany). Thin polycrystalline gold films were prepared by thermal vapor deposition of 100nm gold (99.995%, Chempur) onto polished silicon wafers (Wacker) precovered with a 5 nm titanium adhesion layer. Evaporation was carried out at a pressure of 2×10^{-7}mbar and a deposition rate of 0.5nm/s, yielding a root-mean-square roughness of the Au films

of about 1nm. The gold substrates were kept in an argon atmosphere until use.

Preparation of COOH-Terminated Self-Assembled Monolayers (SAMs)

The 16-mercaptohexadecanoic acid (MHDA, 99%, Aldrich) solution was prepared by dissolving MHDA in a 5% (by volume) solution of acetic acid in ethanol (Merck) to reach the desired concentration of 20μM.[27] A clean gold substrate were placed in this solution for 72h and then rinsed with the pure solvent and gently dried under nitrogen flux.

Fabrication of $Cu_3(BTC)_2$ SURMOFs

All $Cu_3(BTC)_2$ thin films used in the present work were grown on modified Au substrates using the liquid-phase epitaxy (LPE) method, which yields highly oriented and well-defined MOF coatings and can be applied to a variety of substrates. In contrast to the conventional bulk solvothermal MOFs synthesis, where reactants are mixed to initiate the reaction, the layer-by-layer growth of $Cu_3(BTC)_2$ SURMOFs proceeds in two steps comprising a sequential spray solution of the individual reactants. For the present experiments the SURMOFs were grown on a COOH-terminated organic surface on Au.

The SURMOFs were fabricated using the following diluted ethanolic solutions: copper acetate hydrate (1mM, Aldrich) and BTC (1,3,5-Benzenetricarboxylic acid) (0.2mM, Aldrich). For the SURMOF deposition, we used a spray system (Fig S1), as described in detail in an earlier publication.[28] The spray times were 15s for the copper acetate solution and 25s for the BTC solution. Each spray step was followed by a rinsing step (3s) with pure ethanol to remove residual reactants. A total of 20 growth cycles were used for all SURMOFs investigated in this work. Before further experiment, all SURMOF samples were activated by ultrasound in dichloromethane solution for 5min to remove residual solvent from the SURMOF pores and finally checked by XRD.

Characterization of $Cu_3(BTC)_2$ SURMOFs were carried out using X-ray diffraction (XRD) (Fig 1c) and Infrared (IR) spectroscopy (Fig S2). The presence of a broad and strong bands at 1700 -1300 cm^{-1} is assigned to vibrations of COO- of $Cu_3(BTC)_2$.[29] The figure from SEM (Scanning Electron Microscope) picture (Fig S3) show the thickness of SURMOFs is near about 100nm.

Preparation of the $La(OTf)_3@Cu_3(BTC)_2$ SURMOF

First, a $Cu_3(BTC)_2$ thin film on gold substrate was put into 250ml flask and then evacuated to 0.2KPa at room temperature for 30min. Subsequently, the sample was immersed in a freshly prepared solution of $La(OTf)_3$ [lanthanum(III) trifluoromethanesulfonate] in ethanol (1mM, Aldrich) kept at 65°C. After an immersion time of 12h the sample was removed from the solution, rinsed with pure ethanol, and finally dried in a flux of nitrogen gas.

The characteristic R-SO_3^- vibration at 1042cm^{-1} appears after immersing the $Cu_3(BTC)_2$ SURMOFs in a $La(OTf)_3$ solution (Fig S2), this observation provides strong support for the hypothesis presented above, namely, the (OTf) anion is adsorbed in the SURMOFs. Immersing the $La(OTf)_3@Cu_3(BTC)_2$ SURMOF in dichloromethane under ultrasonic condition for 15min, the XRD pattern has no significant change (Fig S4) suggested an irreversible loading of the SURMOF with $La(OTf)_3$.

Modelling

Molecular modeling simulations were performed using a Monte Carlo algorithm implemented in the simulation package SIMONA.[30] In order to avoid the trapping of the system in metastable conformations, basing hopping approach[31-33] with consecutive simulated annealing cycles was used to obtain the lowest energy for the system. Each simulated annealing cycle consists of a series of Metropolis Monte Carlo steps starting at high temperature, where the molecule can escape local minima and traverse energy barriers. Throughout the simulation the temperature is lowered according to:

$$T_n = T_s \cdot c^n, \quad c = \left(\frac{T_E}{T_S}\right)^{\frac{1}{N}} < 1 \qquad (1)$$

Where T_n is the temperature at step n, T_E is the end temperature and N is the total number of steps in simulated annealing run.

The interaction between the atoms was modeled by the classical electrostatic potential:

$$\Phi\left(\vec{r}_i\right) = \frac{1}{4\pi\varepsilon\varepsilon_0}\sum_j^{N_B}\frac{q_i}{r_{ij}} \qquad (2)$$

and the Lennard-Jones interaction which includes terms accounting for van-der-Walls attraction and Pauli repulsion:

$$U_{LJ}(r) = \sum_i^{N_A}\sum_j^{N_B} 4\varepsilon_{ij}\left(\left(\frac{\sigma_{ij}}{r_{ij}}\right)^{12} - \left(\frac{\sigma_{ij}}{r_{ij}}\right)^{6}\right) \qquad (3)$$

We used standard parameters for the Lennard-Jones interaction for all atoms except La. In order to determine the LJ parameters for La^{3+} we performed Metropolis Monte Carlo simulations of La^{3+} with 3(OTf) at constant low temperature (T=1K) and varied the La-parameters until the distance between oxygen and La^{3+} reached the equilibrium distance obtained form ab-initio calculations. The resulting parameters for La^{3+} are epsilon=0.15kcal/mol and sigma=3.425Å. Partial charges were calculated using the ESP fit implemented in the DFT code TURBOMOLE[34] using SV(P) basis and b3-lyp functional (see supplementary information for details, Fig S5).

To screen possible configurations a system consisting of two neighboring cavities (the medium and the large cavity of the MOF) was constructed. Each cavity was loaded with up to four $La(OTf)_3$ molecules resulting in 24 different model systems. To prevent the ions from leaving the complex we applied a strong restraining force to particles outside the cavities:

$$U_{confine}(q) = k(q - x_o)^2,\ q > x_0 \text{ or } q < -x_0,\ q = x, y, z$$

The simulations consisted of 10 simulated annealing runs with N=100000 Metropolis Monte-Carlo steps each, starting at Ts=750K and ending at TE=300K using rigid body translation for La^{3+} and (OTf) and in addition rigid body rotation and rotation around dihedral angles in the (OTf) ions. The step size for the random rigid translations was drawn from a random uniform distribution between 0 and 1Å, the angle of the rigid rotations from a random uniform distribution between 0° and 180°.

Results and discussion, Experimental

Experiments

The out-of-plane XRD data for the pristine HKUST-1 SURMOFs are shown in Fig 1c (black). The (002) and (004) peaks are well-defined and sharp, their relative intensity agrees with that observed for bulk MOF powders and as obtained from simulations using the well-stablished bulk structure of HKSUST-1 (Fig 1a). The absence of diffraction peaks for other crystallographic directions in the out-of-plane data reveals that that the SURMOF growth proceeds only along the (001) direction on the MHDA SAM. The in-plane XRD data only show the (200) and (220) direction also supports this orientation structure (Fig 1c red). XRD data recorded after immersion into the $La(OTf)_3$ solution are shown in Fig 1c (out-of-plane, blue; in-plane, dark yellow). No new diffraction peaks appeared revealing that the structure of the MOF lattice has remained unchanged. However, the form factor is strongly different, after loading the ratio of (002)/(004) (out-of-plane data) has decreased from 1.1 for the pristine film to 0.7 for the La loaded film. Also the in-plane XRD data reveal pronounced changes: the ratio of (200)/(400) has dropped from 1.6 to 0.1. Longer immersion times did not lead to a further change of the relative XRD peak intensities.

The same loading process has also been carried out for powder $Cu_3(BTC)_2$ MOF. The changes of relative peak intensities observed for the powders were similar to that seen for the SURMOFs (Fig S6). The ratio of (002)/(004) has dropped from 2.15 to 1.21 when after loading $La(OTf)_3$.

This significant change in relative intensities of XRD-peaks directly demonstrates that La^{3+} ions are loaded in virtually every pore of the SURMOF (and MOF powders), a decoration of the outer surface only would not be compatible with the change of diffraction peak relative intensities.

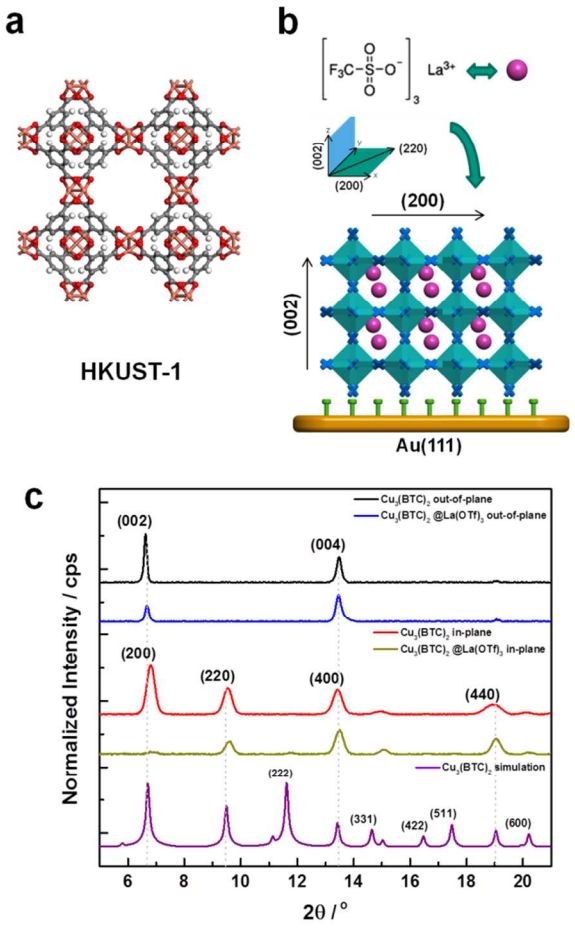

Fig. 1 (a) Schematic structure of $Cu_3(BTC)_2$ (HKUST-1). (b) Schematic structure of $Cu_3(BTC)_2$ MOF thin films grown on a MHDA SAM after loading $La(OTf)_3$. (c) X-ray diffraction patterns recorded: calculated XRD pattern for $Cu_3(BTC)_2$ with a bulk structure (purple) and experimental XRD data recorded in out-of-plane [empty $Cu_3(BTC)_2$ (black) and after loading $La(OTf)_3$ (blue)] and in-plane [empty $Cu_3(BTC)_2$ (red) and after loading $La(OTf)_3$ (dark yellow)] scattering geometry.

The results of the XPS analysis are shown in Fig 2. Clearly, after loading the data recorded for of the $La(OTf)_3@Cu_3(BTC)_2$ SURMOFs show distinctive La peaks.[35] A quantitative analysis reveals that the total copper and lanthanum content of the SURMOFs after loading are 4.3% and 0.8%, respectively (Table S2).

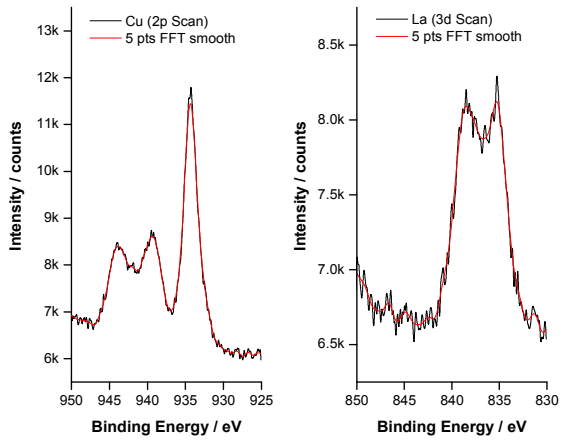

Fig. 2 X-ray photoelectron spectrum (XPS) of (a) Cu 2p and (b) La 3d of the $La(OTf)_3@Cu_3(BTC)_2$ MOF thin films.

The metal ions concentration curves from inductively coupled plasma optical emission spectrometry (ICP-OES) measurement are shown in Fig 3. By calculation of the integrated area of the measure curves, the copper and lanthanum concentration after loading sample are 6.6mg/L and 0.9mg/L, respectively (Table S3), the calculated ratio of Cu/La amounts to 7.3:1, which is closed to the value calculated from XPS data.

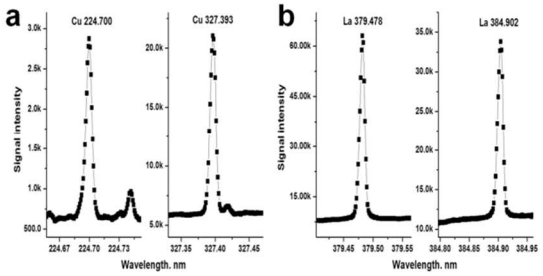

Fig. 3 Inductively Coupled Plasma Optical Emission Spectrometry (ICP-OES) of (a) Cu^{2+} and (b) La^{3+} of the $La(OTf)_3@Cu_3(BTC)_2$ MOF thin films.

Simulations

In order to complement the experimental data to obtain detailed information regarding the positions of the molecules within the MOF pores we have carried out force-field based Monte Carlo simulations for different numbers of $La(OTf)_3$ embedded in $Cu_3(BTC)_2$. First, simulations of up to four $La(OTf)_3$ moieties within a single $Cu_3(BTC)_2$ unit cell were performed and the binding energies were calculated. To confine the $La(OTf)_3$ moieties to the cavity an additional harmonic penalty potential (confining potential) was introduced for particles outside the cavity. Results for binding energies and the confining harmonic potential of the lowest energy state are displayed in table 1. The binding energy is decreasing with an increase of the number of moieties for up to four molecules, as repulsive interactions between the molecules compete with attractive interactions to the MOF. We note that the confining potential at the energy minimum is increased significantly when more than three $La(OTf)_3$ are loaded in each per cavity, which indicates that no more than 3 molecules can fit one pore. There is a substantial binding energy associated with the loading, which mainly results from out by the dispersive interaction of the La^{3+} ion, which is moved close to the center phenyl ring of one of the BTC ligands at the energy minimum (Fig S7). Because this interaction may not be fully represented in the force field, we have performed additional DFT calculations to obtain the binding between La^{3+} and the phenyl rings and obtained a binding energy of -7.84 eV which is approximately 300 times kBT at room temperature.

In order to compare with the experimental data both cavities were loaded with different numbers of $La(OTf)_3$ and simulation with 10 SA-cycles with 100000 MC steps each, starting at T=750K and cooling down to T=300K, were carried out. The optimized structure with possible locations and number (1, 2, 3, 4) of $La(OTf)_3$ in the large pore of $Cu_3(BTC)_2$ MOF is presented in Fig 4a and Fig S6. The simulated out-of-plane XRD data for a (001) growth direction for the optimized structures obtained from the calculations are shown in Fig 4b.

The increase of the (004) peak relative to the (002) peak in the calculated XRD data when adding the first La ion close to the Cu^{2+} ions can be rationalized by considering the fact that this structure can (to first approximation) be described as an F lattice, and the intensity of the (002) peaks has to increase because placing the La^{3+} ion close to the Cu ions effectively increases the electron density around these Cu position is increased. When additional La^{3+} ions are placed more close to the middle of the major pore (as in the structures for the 2 and 3 ions by the structure optimizations) the F-lattice is effectively changed into an I-lattice (Fig S6). The extinction rules for I-lattices lead to a decrease of the (002) peak intensity, as it is evident in the figure for the case of 2 and 3 La^{3+} ions. Further increase of the La content in the unit cell leads to an increase of the intensity. This can be explained by the higher atomic scattering factor of the La and its position. The former Cu F-lattice transforms into a La F-lattice (or even P-lattice) with some admixtures of Cu in the I-lattice positions. The atomic scattering factor for Cu cannot fully compensate the La contributions to the scattered intensity. The effect explaining the intensity decrease for the 1La and 2La loading state applies also for the higher loading states for La, hence, a initial Cu dominated structure is no transformed into a La dominated structure. This result is fit very well with the experiment data. The results for the two and three ions are very similar in the out-of-plane data.

Table 1 Binding energies and confining potential for numbers (1, 2, 3, 4) of $La(OTf)_3$ molecular in a single MOF cavity.

$Cu_3(BTC)_2$ of $La(OTf)_3$	binding energy / kcal / mol	confining potential
1	-837.33	6.53
2	-1235.38	49.08
3	-1482.21	47.34
4	-1559.74	152.89

By comparing with the results of structure optimizations, loading with a single La ion can be ruled out because for the poor agreement of the simulated with the experimental XRD data. On the other hand a loading with 3 ions per HKUST-1 unit cell can be ruled out because of the poor agreement with the ICP-OES data. We thus conclude that in the loaded structure $2La^{3+}$ ions are hosted within the pore of $Cu_3(BTC)_2$. This finding is fully consistent with all available experimental and theoretical information.

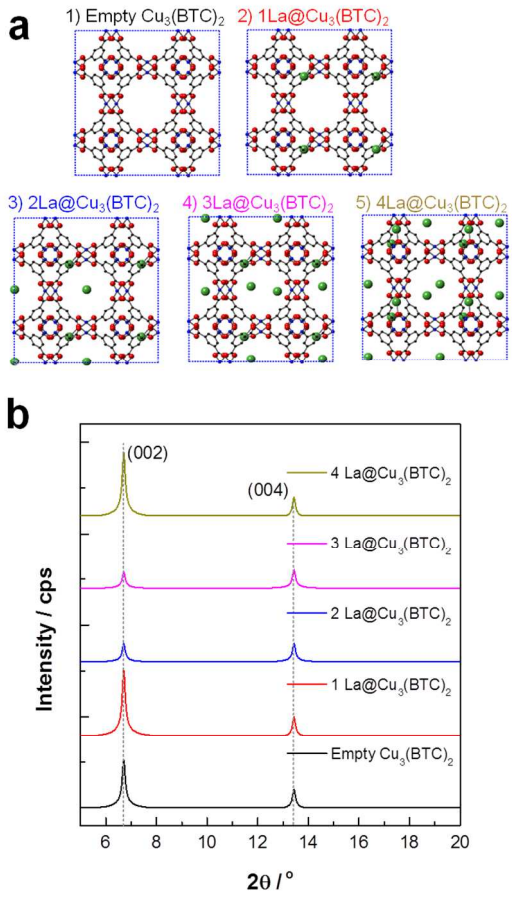

Fig. 4 (a) Schematic structure of $Cu_3(BTC)_2$ (1) and after loading different number [single $La(OTf)_3$ (2), 2 $La(OTf)_3$ (3) , 3 $La(OTf)_3$ (4) and 4 $La(OTf)_3$ (5)] of $La(OTf)_3$ in $Cu_3(BTC)_2$. (b) Calculated X-ray diffraction patterns for $Cu_3(BTC)_2$ before and after loading $La(OTf)_3$ molecular in out-of-plane [empty $Cu_3(BTC)_2$ (black), single $La(OTf)_3$ (red), 2 $La(OTf)_3$ (blue), 3 $La(OTf)_3$ (magenta) and 4 $La(OTf)_3$ (dark yellow)].

Conclusions

In conclusion, $La(OTf)_3$ was successful loaded into $Cu_3(BTC)_2$ SURMOF via solution impregnation method as evidenced by XPS, ICP-OES and IR data. By additionally considering the results of theoretical structure optimizations using a refined force-field analysis, we find a loading with two La-ions per unit cell to give the best agreements. This structure is stabilized by pronounced dispersive interactions between the La ion and the phenyl ring of a BTC ligand. The resultant loading of La (and other noble metal) species into the porous solid is of pronounced interest with regard to using MOF thin films for applications. Loading with metal ions and subsequently using redox-chemistry to create new species inside the MOF has recently created substantial attention in the context of information storage.[19] In future work we plan to study the electrochemical properties of the loaded SURMOFs also offers rich potential for catalysis applications.

Acknowledgements

We thank Vanessa Trouillet (Institute for Applied Materials – Energy Storage Systems (IAM-ESS), Karlsruhe Institute of Technology, Germany) for the XPS measurement, Marita Heinle (Institute of Functional Interfaces (IFI), Karlsruhe Institute of Technology, Germany)) for the ICP-OES measurements and Stefan Heißler (Institute of Functional Interfaces (IFG), Karlsruhe Institute of Technology, Germany) for the fluorescence measurements. Financial support by Deutsche Forschungsgemeinschaft (DFG) within the Priority Program Metal Organic Frameworks (SPP 1362) is gratefully acknowledged. The authors acknowledge the financial support of the Chinese Scholarship Council (CSC).

Notes and references

[a] Karlsruhe Institute of Technology, Institute of Functional Interfaces (IFG), Hermann-von-Helmholtz-Platz 1, 76344 Eggenstein-Leopoldshafen, Germany
E-mail: christof.Woell@kit.edu; Fax: +49-(0)721-608-23478; Tel: +49-(0)721-608-23775
[b] Karlsruhe Institute of Technology, Institute of Nanotechnologie (INT), Hermann-von-Helmholtz-Platz 1, 76344 Eggenstein-Leopoldshafen, Germany
[c] Karlsruhe Institute of Technology, Institute of Inorganic Chemistry, Engesserstraße 15, 3. OG, Room 330, 76344 Karlsruhe, Germany
† Electronic Supplementary Information (ESI) available: See DOI: 10.1039/b000000x/

1 H. Li, M. Eddaoudi, M. O'Keeffe and O. M. Yaghi, *Nature*, 1999, 402, 276-279.
2 R. Makiura, S. Motoyama, Y. Umemura, H. Yamanaka, O. Sakata and H. Kitagawa, *Nature Materials*, 2010, 9, 565-571.
3 C. Mellot-Draznieks, J. Dutour and G. R. Ferey, *Angew. Chem.-Int. Edit.*, 2004, 43, 6290-6296.
4 J. Liu, B. Lukose, O. Shekhah, H. K. Arslan, P. Weidler, H. Gliemann, S. Braese, S. Grosjean, A. Godt, X. Feng, K. Muellen, I.-B. Magdau, T. Heine and C. Wöll, *Sci Rep-Uk*, 2012, 2.
5 M. Meilikhov, K. Yusenko, D. Esken, S. Turner, G. Van Tendeloo and R. A. Fischer, *Eur J Inorg Chem*, 2010, 3701-3714.
6 D. Esken, S. Turner, O. I. Lebedev, G. Van Tendeloo and R. A. Fischer, *Chem. Mat.*, 2010, 22, 6393-6401.
7 D. Esken, H. Noei, Y. M. Wang, C. Wiktor, S. Turner, G. Van Tendeloo and R. A. Fischer, *J. Mater. Chem.*, 2011, 21, 5907-5915.
8 D. Esken, X. Zhang, O. I. Lebedev, F. Schroder and R. A. Fischer, *J. Mater. Chem.*, 2009, 19, 1314-1319.
9 S. Proch, J. Herrmannsdorfer, R. Kempe, C. Kern, A. Jess, L. Seyfarth and J. Senker, *Chemistry-a European Journal*, 2008, 14, 8204-8212.
10 S. J. Yang, J. H. Cho, K. S. Nahm and C. R. Park, *Int J Hydrogen Energ*, 2010, 35, 13062-13067.
11 J. Y. Ye and C. J. Liu, *Chem. Commun.*, 2011, 47, 2167-2169.
12 H. L. Jiang, B. Liu, T. Akita, M. Haruta, H. Sakurai and Q. Xu, *J. Am. Chem. Soc.*, 2009, 131, 11302-+.
13 T. Ishida, M. Nagaoka, T. Akita and M. Haruta, *Chemistry-a European Journal*, 2008, 14, 8456-8460.

14 A. A. Talin, A. Centrone, A. C. Ford, M. E. Foster, V. Stavila, P. Haney, R. A. Kinney, V. Szalai, F. El Gabaly, H. P. Yoon, F. Leonard and M. D. Allendorf, *Science*, 2014, 343, 66-69.
15 J. He, M. Q. Zha, J. S. Cui, M. Zeller, A. D. Hunter, S. M. Yiu, S. T. Lee and Z. T. Xu, *J. Am. Chem. Soc.*, 2013, 135, 7807-7810.
16 S. Y. Jin, H. J. Son, O. K. Farha, G. P. Wiederrecht and J. T. Hupp, *J. Am. Chem. Soc.*, 2013, 135, 955-958.
17 E. Redel, Z. B. Wang, S. Walheim, J. X. Liu, H. Gliemann and C. Wöll, *Applied Physics Letters*, 2013, 103.
18 M. D. Allendorf, A. Schwartzberg, V. Stavila and A. A. Talin, *Chemistry-a European Journal*, 2011, 17, 11372-11388.
19 S. M. Yoon, S. C. Warren and B. A. Grzybowski, *Angew. Chem.-Int. Edit.*, 2014, 53, 4437-4441.
20 A. Dragasser, O. Shekhah, O. Zybaylo, C. Shen, M. Buck, C. Wöll and D. Schlettwein, *Chem. Commun.*, 2012, 48, 663-665.
21 X. W. Dong, T. Liu, Y. Z. Hu, X. Y. Liu and C. M. Che, *Chem. Commun.*, 2013, 49, 7681-7683.
22 O. Shekhah, J. Liu, R. A. Fischer and C. Wöll, *Chem. Soc. Rev.*, 2011, 40, 1081-1106.
23 H. Gliemann and C. Wöll, *materials today*, 2012, 15, 110-116.
24 S. Bundschuh, O. Kraft, H. K. Arslan, H. Gliemann, P. G. Weidler and C. Wöll, *Applied Physics Letters*, 2012, 101.
25 H. C. Streit, M. Adlung, O. Shekhah, X. Stammer, H. K. Arslan, O. Zybaylo, T. Ladnorg, H. Gliemann, M. Franzreb, C. Wöll and C. Wickleder, *ChemPhysChem*, 2012, 13, 2699-2702.
26 S. S. Y. Chui, S. M. F. Lo, J. P. H. Charmant, A. G. Orpen and I. D. Williams, *Science*, 1999, 283, 1148-1150.
27 M. Kind and C. Wöll, *Prog. Surf. Sci.*, 2009, 84, 230-278.
28 H. K. Arslan, O. Shekhah, J. Wohlgemuth, M. Franzreb, R. A. Fischer and C. Wöll, *Advanced functional materials*, 2011, 21, 4228-4231.
29 O. Zybaylo, O. Shekhah, H. Wang, M. Tafipolsky, R. Schmid, D. Johannsmann and C. Wöll, *Phys. Chem. Chem. Phys.*, 2010, 12, 8092-8097.
30 T. Strunk, M. Wolf, M. Brieg, K. Klenin, A. Biewer, F. Tristram, M. Ernst, P. J. Kleine, N. Heilmann, I. Kondov and W. Wenzel, *J Comput Chem*, 2012, 33, 2602-2613.
31 S. Kirkpatrick, C. D. Gelatt and M. P. Vecchi, *Science*, 1983, 220, 671-680.
32 Z. Q. Li and H. A. Scheraga, *Proc. Natl. Acad. Sci. U. S. A.*, 1987, 84, 6611-6615.
33 D. J. Wales and H. A. Scheraga, *Science*, 1999, 285, 1368-1372.
34 R. Ahlrichs, M. Bar, M. Haser, H. Horn and C. Kolmel, *Chemical Physics Letters*, 1989, 162, 165-169.
35 V. V. Atuchin, A. V. Kalinkin, V. A. Kochubey, V. N. Kruchinin, R. S. Vemuri and C. V. Ramana, *J Vac Sci Technol A*, 2011, 29.